



RESEARCH ARTICLE

10.1029/2024JD041621

E. Boutsoukidis and E. Germain-Piaulenne these authors contributed equally to this work.

Attribution of Excess Methane Emissions Over Marine Environments of the Mediterranean and Arabian Peninsula

E. Boutsoukidis¹ , E. Germain-Piaulenne^{1,2}, V. Gros² , P.-Y. Quéhé¹, M. Pikridas¹, J. Byron³, J. Williams^{1,3}, D. Gliddon⁴ , R. Mohamed⁴, R. Ekaabi⁴, J. Lelieveld^{1,3} , J. Sciare¹ , O. Teixidó⁵ , and J.-D. Paris^{1,2} 

¹Climate and Atmosphere Research Center (CARE-C), The Cyprus Institute, Nicosia, Cyprus, ²Laboratoire des Sciences du Climat et de l'Environnement (LSCE), CEA-CNRS-UVSQ, IPSL, Guyancourt, France, ³Max Planck Institute for Chemistry (MPIC), Mainz, Germany, ⁴Environment Agency - Abu Dhabi (EAD), Abu Dhabi, United Arab Emirates, ⁵Ricardo plc., Abu Dhabi, United Arab Emirates

Key Points:

- The Suez Canal and the Gulf of Suez are regional pollution hotspots with underestimated methane emission sources
- Discrepancies between observed and modeled methane mixing ratios were resolved using non-methane hydrocarbon observations
- Methane sources from the oil and gas exploitation sector in the Middle East are particularly uncertain in emission inventories

Supporting Information:

Supporting Information may be found in the online version of this article.

Correspondence to:

E. Boutsoukidis,
e.boutsoukidis@cyi.ac.cy

Citation:

Boutsoukidis, E., Germain-Piaulenne, E., Gros, V., Quéhé, P.-Y., Pikridas, M., Byron, J., et al. (2024). Attribution of excess methane emissions over marine environments of the Mediterranean and Arabian Peninsula. *Journal of Geophysical Research: Atmospheres*, 129, e2024JD041621. <https://doi.org/10.1029/2024JD041621>

Received 21 MAY 2024

Accepted 12 SEP 2024

Author Contributions:

Conceptualization: E. Boutsoukidis, E. Germain-Piaulenne, V. Gros, J. Lelieveld, J. Sciare, O. Teixidó, J.-D. Paris

Data curation: E. Boutsoukidis, E. Germain-Piaulenne, P.-Y. Quéhé, M. Pikridas, J. Byron

Formal analysis: E. Boutsoukidis, E. Germain-Piaulenne, P.-Y. Quéhé, M. Pikridas, J. Byron, J.-D. Paris

© 2024. The Author(s).

This is an open access article under the terms of the [Creative Commons Attribution License](https://creativecommons.org/licenses/by/4.0/), which permits use, distribution and reproduction in any medium, provided the original work is properly cited.

Abstract To accurately assess the current atmospheric methane budget and its future trends, it is essential to apportion and quantify the anthropogenic methane emissions to specific sources. This poses a significant challenge in the under-sampled Middle East, where estimates predominantly depend on remote sensing observations and bottom-up reporting of national emissions. Here, we present *in situ* shipborne observations of greenhouse gases (GHGs) and non-methane hydrocarbons (NMHCs) collected along a >10,000-km route from Vigo, Spain, to Abu Dhabi, UAE. By comparing our observations with Lagrangian dispersion model simulations, coupled with two methane emission inventories, we identify periods of considerable mismatch and apportion the responsible sources. Employing interspecies relationships with NMHCs has enabled the characterization of methane emissions from oil and gas (O&G) operations, urban centers, Red Sea deep water, enteric fermentation, and agriculture across diverse atmospheric environments. Our analysis reveals that the Suez area is a regional emission hotspot, where simulations consistently underestimate the methane emission sources. Importantly, the Middle Eastern O&G sector has been identified as an additional source of considerable uncertainty. Here, methane emissions were alternately underestimated and overestimated by the two inventories, exposing significant gaps in our understanding of fuel exploitation-related emissions in the Middle East. This underscores the need for further targeted field campaigns and long-term observations to improve the accuracy of emission data in the inventories.

Plain Language Summary For the mitigation of human-induced methane emissions, a detailed characterization of its numerous sources is vital. This is particularly challenging in understudied regions where the source attribution and emission strength thus far relies on satellite observations and country reports. Although such data, representing the entire atmospheric column, are invaluable, source specific emission estimates remain highly uncertain. In this study, we used shipborne measurements of methane to evaluate the performance of two emission inventories commonly used in computer-based models to simulate methane atmospheric concentrations. The relationships between methane and various co-emitted reactive trace gases revealed the causes of discrepancies between observations and model simulations. Our results show that, while models are generally reliable at capturing high methane concentrations, they are deficient in the Suez and Middle East areas due to inadequate characterization of emissions from Oil and Gas operations. The research outcomes of this study underscore the crucial role of ground-based observations in improving the accuracy of methane emission inventories and their reporting, and in supporting evidence-based policies to mitigate climate change and improve air quality.

1. Introduction

Anthropogenic emissions of methane (CH₄) have contributed approximately +0.5°C to climate warming since pre-industrial times (Lee et al., 2023). With a high global warming potential 28 times that of carbon dioxide (CO₂) and an atmospheric lifetime of about 9 years, methane has emerged as a critical target for immediate climate mitigation efforts (Ocko et al., 2021). Anthropogenic activities contribute to over 50% of global methane emissions (Saunio et al., 2024), with agriculture and waste management accounting for 38% and the production and utilization of fossil fuels accounting for 18%. Notably, two-thirds of these fossil fuel-related methane emissions originate from oil and gas (O&G) exploitation operations (IEA, 2024). These emissions occur at

Funding acquisition: D. Gliddon, R. Mohamed, R. Ekaabi, J. Lelieveld, J. Sciare, O. Teixidó
Investigation: E. Bourtsoukidis, E. Germain-Piaulenne, V. Gros, J. Byron, J.-D. Paris
Methodology: E. Bourtsoukidis, E. Germain-Piaulenne, P.-Y. Quéhé, J.-D. Paris
Project administration: V. Gros, M. Pikridas, D. Gliddon, R. Mohamed, R. Ekaabi, J. Lelieveld, J. Sciare, O. Teixidó
Resources: J. Williams, D. Gliddon, R. Mohamed, R. Ekaabi, J. Lelieveld, J. Sciare, O. Teixidó
Software: E. Bourtsoukidis, E. Germain-Piaulenne, P.-Y. Quéhé, M. Pikridas, J.-D. Paris
Supervision: E. Bourtsoukidis, V. Gros, J. Sciare, J.-D. Paris
Validation: E. Bourtsoukidis, E. Germain-Piaulenne, V. Gros, J. Byron
Visualization: E. Bourtsoukidis, E. Germain-Piaulenne, M. Pikridas
Writing – original draft: E. Bourtsoukidis, E. Germain-Piaulenne, V. Gros
Writing – review & editing: P.-Y. Quéhé, M. Pikridas, J. Byron, J. Williams, D. Gliddon, R. Mohamed, R. Ekaabi, J. Lelieveld, J. Sciare, O. Teixidó, J.-D. Paris

various stages of the O&G supply chain, including extraction, production, refining, and transportation, in addition to leaks, venting, or flaring (Alvarez et al., 2018). Over the last few years, international efforts have been focused to accelerate action on methane. Several significant initiatives were launched at the COP 28 climate summit in Dubai. Over 50 oil and gas companies have introduced the Oil and Gas Decarbonization Charter (OGDC) to expedite emission reductions within the industry. Additionally, more countries have joined the Global Methane Pledge, and new funding has been secured to support the reduction of methane and other greenhouse gases besides carbon dioxide (CO₂) (IEA, 2024).

The high variability and dynamic nature of methane emission sources pose significant challenges that are typically addressed through the integration of reported emission factors, activity data, and modeling approaches. This integration facilitates a more precise spatiotemporal estimation of the emissions. Emission inventories such as the widely adopted Emissions Database for Global Atmospheric Research (EDGAR) and Evaluating the Climate and Air Quality Impact of Short-Lived Pollutants (ECLIPSE) provide detailed annual and sectoral emission estimations worldwide that range from country-level factors to spatial resolutions as fine as 0.1 × 0.1° grid cells (Höglund-Isaksson, 2012; Janssens-Maenhout et al., 2019; Upadhyay et al., 2020). Despite advancements in emission estimation methods, these inventories are still associated with uncertainties that stem from variability in emission factors, the precision and accessibility of activity data, limited monitoring and reporting requirements by countries, the incomplete representation of emission sources, and the complex patterns of emission signatures (Alvarez et al., 2018; Chen et al., 2019; McNorton et al., 2018; Zavala-Araiza et al., 2015).

The challenge of creating an accurate methane emissions database is particularly acute in global O&G hotspots with poor data coverage, such as in the Middle East. This region's sectoral emissions have increased by 32% for fossil fuels (>80% O&G) and by 26% for agriculture and waste within the period 2008–2017 (Stavert et al., 2022). Over the past decade, several studies in this region have uncovered substantial inconsistencies among top-down estimates, inventory-based estimates, and direct atmospheric observations (Germain-Piaulenne et al., 2024; Maasackers et al., 2019; Paris et al., 2021; Stavert et al., 2022; Turner et al., 2019; Zavala-Araiza et al., 2015). While the waste management sector is recognized as a substantial source of methane emissions in the region (Al-Shalan et al., 2022), the Middle East's significant role in global oil production—accounting for 32% of the world's crude oil (OPEC, 2020)—highlights the uncertainties in methane emissions along the production line. Satellite-based observations have identified new O&G super-emitters in the northeastern Middle East, albeit fewer in numbers than initially anticipated across the region. Furthermore, isotopic analyses have revealed a 60%–100% underestimation of the methane emissions from the O&G sector (Schwietzke et al., 2016), indicating significant discrepancies in inventory methodologies. Despite the upward revision of the emissions from the O&G sector, an underestimation of the Middle Eastern oil extraction-related methane emissions has still been identified from a shipborne campaign in the Arabian Gulf (Paris et al., 2021). The emissions from the fuel exploitation sector in the Arabian Peninsula are still affected by uncertainties that are larger than 20% (Stavert et al., 2022; Tibrewal et al., 2024) since the quantification of the methane emissions from this sector is challenging, with top-down estimates tending to overestimate, while bottom-up approaches tend to underestimate the observations (Cooper et al., 2022). The overall magnitude of methane emissions from all anthropogenic sources is actively debated, with bottom-up analyses differing from top-down analyses by 50% or more (Allen, 2016).

With atmospheric lifetimes ranging from days to weeks (Parrish et al., 2007), non-methane hydrocarbons (NMHC) measurements are increasingly utilized to identify methane sources. For example, the ratio between ethane (C₂H₆) and methane and the pentane isomer ratio (i/n-C₅H₁₂) have been previously used to apportion an O&G-related emission signal (Bourtsoukidis et al., 2019; Germain-Piaulenne et al., 2024; Gilman et al., 2013; Paris et al., 2021; Wilde et al., 2021; Yacovitch et al., 2020). When these ratios are combined with Lagrangian modeling to predict long-range transport and dispersion of atmospheric pollutants (Stohl et al., 2005), the emission inventories can be evaluated with reasonable accuracy. Such an approach aids in pinpointing discrepancies between predicted and observed concentrations, thereby identifying sources of uncertainty that can help refine the emission inventory estimates.

In this study, we present observations of methane and NMHCs collected during the Atmospheric Research Expedition to Abu Dhabi (AREAD) shipborne campaign in the winter of 2022. By comparing these observational data with simulations from Lagrangian dispersion models and analyzing relationships with NMHCs, we refine our understanding of methane emissions in the Middle East and identify the causes of potential discrepancies. Ultimately, this study delivers an *in situ* measurement-based analysis of the Mediterranean and Middle Eastern

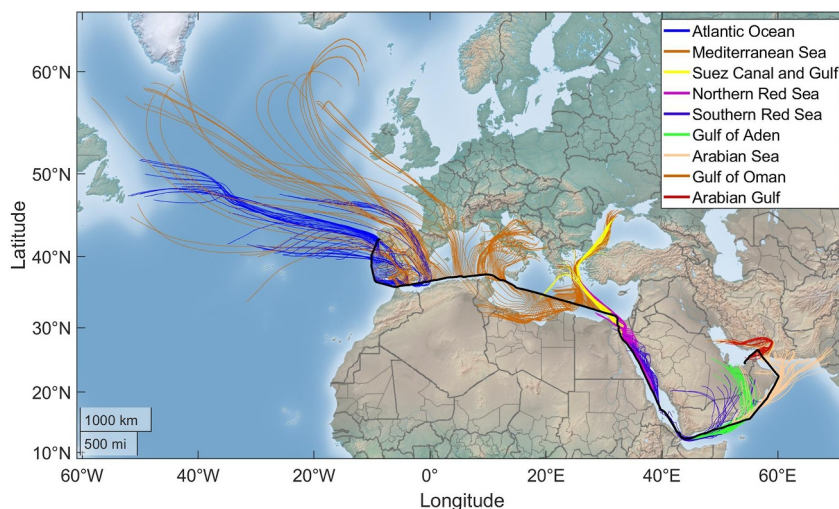


Figure 1. The map shows the ship's track (in black) and the geographical areas used in the analysis. The hourly back trajectories (72 hr back) are color-coded, as defined in the insert, to indicate the origin and path of air masses encountered during the campaign.

marine environments, aiming to evaluate the precision with which methane emissions are attributed to various sectors in these under-researched regions.

2. Research Design and Methods

2.1. The AREAD Ship Campaign

The Atmospheric Research Expedition to Abu Dhabi (AREAD) was conducted in winter 2022 aboard the Jaywun research vessel owned and operated by the Environment Agency—Abu Dhabi (EAD). With a length of 47 m and beam of 12 m, the vessel was equipped with an array of gas-phase and aerosol instruments installed at the ship's forefront to minimize possible contamination from the ship stack. The expedition aimed to study the atmospheric composition and chemical processes over the poorly studied Eastern Mediterranean and Arabian Peninsula, regions notably affected by climate change and atmospheric pollution (Osipov et al., 2022; Zittis et al., 2022). Throughout the campaign, the vessel navigated 10,147 km with an average speed of 11.0 ± 8.6 km/hr. The voyage commenced in Vigo, Spain, on November 25th and concluded in Abu Dhabi, United Arab Emirates (UAE), on 20 December (Figure 1). The route of the ship route was divided into geographical sectors, resembling those chosen for the Air Quality in the Arabian Basin (AQABA) ship campaign which occurred in the summer of 2017 and followed a similar route (Bourtsoukidis et al., 2019). The exact coordinates, days of sampling, and the number of collected samples are provided in Table S1 in Supporting Information S1.

Meteorological conditions were continuously monitored using a weather station (Airmar 150WX; Airmar Technology Corporation, USA) located on the vessel's front deck, near the air sampling inlets. Average temperature ($^{\circ}\text{C}$), relative humidity (%), and wind conditions (speed in m/s and direction in degrees) were calculated for the different subregions (Table S2 in Supporting Information S1). Throughout the expedition, temperatures ranged from 8.6 to 32.6°C , averaging $19.2 \pm 5.2^{\circ}\text{C}$. Relative humidity reached 87.4% , averaging $47.0 \pm 31.1\%$, while wind speeds were observed between 0.1 and 51.2 m/s, with an average of 4.9 ± 4.7 m/s.

2.2. Experimental Setup

2.2.1. Greenhouse Gases

Methane (CH_4), carbon dioxide (CO_2), and carbon monoxide (CO) mixing ratios were measured using a Picarro analyzer G2401 (Picarro Inc. USA) employing cavity ring-down spectroscopy. The analyzer, previously evaluated for precision and repeatability according to the Integrated Carbon Observation System—Atmosphere Thematic Center (ICOS-ATC) protocol (Yver Kwok et al., 2015), achieved minute-averaged precision (1σ) values of 0.1 , 0.73 , and 12 ppb for CH_4 , CO , and CO_2 , respectively. Two filters were installed before the

instrument's inlet: a ceramic filter with 2 μm porosity (M&C, Germany) and an all-welded stainless steel filter with 0.5 μm porosity (Swagelok, USA). The M&C filter is designed with a shaped glass bowl, which also functions as a water trap. Laboratory-determined water vapor corrections were also applied to the data acquisition (Rella et al., 2013). Linear calibrations using four compressed gas cylinders were performed both at the beginning and end of the campaign and showed good stability with a standard deviation for CH_4 of 0.08 ppb. Daily injections of a WMO-scale-traceable target gas (provided by ICOS-ATC) with known mixing ratios (2036.9 ppb CH_4 , 323.1 ppb CO , and 446.2 ppm CO_2) were part of the frequent quality control measures. The processing and quality control of raw data followed the standard procedure of the Integrated Carbon Observing System (ICOS) Atmosphere Thematic Center.

2.2.2. Non-Methane Hydrocarbons

Non-methane Hydrocarbons (C2–C6) were measured using an automated Gas Chromatograph—Flame Ionization Detector (GC-FID; AMA Instruments GmbH, Germany). The analyzer and operating principle of the GC-FID were identical to those used during the AQABA ship campaign in 2017. Details regarding the operational protocol, including instrument-related sampling flows and volumes, preconcentration of NMHCs, oven settings, column characteristics, and the calibration approach, can be found in Bourtsoukidis et al. (2019). The only notable change from the previously reported setup was in the inlet system. During AREAD, NMHCs were drawn at a flow rate of 190 sccm through a heated (40°C) ¼-inch Teflon line of 6 m length, resulting in a residence time in the sampling line of approximately 22 s. To ensure artifact-free sampling, a Nafion dryer and a Teflon (PTFE) filter (5 μm pore size, Sartorius Corporate Administration GmbH, Germany) were employed for particle removal, while ozone was removed through an ozone scrubber ($\text{Na}_2\text{S}_2\text{O}_3$ -infused quartz filters) at the sampling inlet entrance.

2.2.3. Ship Exhaust Flag

Although the measurement inlets were positioned at the bow of Jaywun, the ship's emissions occasionally impacted the measurements, depending on the relative directions of the wind and the course of the ship. To address this contamination issue, we implemented a minute-by-minute visual data screening using wind data along with observations of CO , ozone (O_3), nitrogen oxides (NO_x), sulfur dioxide (SO_2), and total aerosol particle number concentrations. Figure S1 in Supporting Information S1 illustrates examples of the ship exhaust flagging for 2 days that include the entrance and the crossing of the Suez Canal. This method identified 14% of the data as contaminated by the ship exhaust. Consequently, our analyses excluded affected measurements.

2.3. Lagrangian Dispersion Model Simulations

To investigate the atmospheric transport characteristics, particularly the origins of air masses influencing the measurements on the ship, the Lagrangian FLEXible PARTicle dispersion model was used. The model calculates the trajectories of 10,000 particles per release, which occurs every three hours or for each $0.1 \times 0.1^\circ$ grid cell. Each trajectory was tracked backward in time for 10 days, using mean wind fields from the ECMWF ERA5 at a 1° resolution across the Northern Hemisphere. We used ERA5 data from ECMWF at a resolution of $0.5^\circ \times 0.5^\circ$ and 3-hr intervals. ECMWF meteorological data were retrieved and formatted using the FLEX-extract toolbox and FLEXPART simulations were performed within the GUI toolbox (Berchet et al., 2023). A good correlation ($r = 0.62$, $p < 10^{-15}$) was found between the wind fields used to drive the model and the observed wind direction (Figure S2 in Supporting Information S1) at the ship position. A particle residence time below 500 m defines the Potential Emission Sensitivity (PES), which can be combined with gridded surface fluxes from inventories to simulate species excess by the sector and the region at any given ship position.

As concluded by an intercomparison of atmospheric trace gas dispersion models (Karion et al., 2019), uncertainties in these models, particularly related to vertical and horizontal dispersion processes and meteorological conditions, can significantly impact the accuracy of emission estimates. In our study, while we have mitigated some of these uncertainties by employing high-resolution ERA5 data and optimizing particle release parameters, the inherent limitations of the FLEXPART model, especially in regions with complex meteorology, must be considered when interpreting our results. These limitations are particularly relevant in areas with rapidly changing atmospheric conditions, such as over the Suez Canal (Fiocco et al., 1980), where the model's ability to accurately simulate the transport and dispersion of gases is not optimal. In addition, there are uncertainties related to the definition of the chemical background. However, these are better mitigated due to FLEXPART's ability to

integrate 3D methane mixing ratio fields with trajectory positions, which refines our chemical background definition and addresses the sensitivity of our results to the 10-day back trajectory length. The geographical regions are defined as West Europe (−10 to 26°E, 34 to 60°N), East Europe with Turkey and Russia (26–60°E, 36 to 60°N), North Africa (−10 to 35°E, 10 to 34°N), Middle East (35–60°E, 10 to 36°N), and other regions which correspond to influence outside of the aforementioned regions. The inventory used was EDGAR v7 for 2021, which provides the country's total methane emissions, among other species, on a yearly basis at a $0.1 \times 0.1^\circ$ resolution with 26 emission sectors derived from international emission factors and activity data. The simulated excess in mixing ratios at the receptor (C) from the CH_4 flux in each grid cell was calculated as follows:

$$C = \sum(x) [\text{PES}(x) * (\text{Flux}(x) * 1000) * (M_{\text{air}}/M_{\text{CH}_4})] \quad (1)$$

with PES expressed in ppb ($\text{g m}^{-2} \text{s}^{-1}$)^{−1}, flux from the EDGAR database in $\text{kg m}^{-2} \text{s}^{-1}$, and the M_{air} and M_{CH_4} the air and CH_4 molar masses, respectively, and x being any grid cell.

2.4. Definition of Excess Mixing Ratios

The excess mixing ratio of species X above the background levels is defined as follows:

$$\Delta[X] = [X] - [X]_{\text{bg.}} \quad (2)$$

where X represents the species of interest. In this study, the excess mixing ratios for CH_4 , CO_2 , CO , and ethane were calculated. The background (bg.) for species X is defined as the rolling average of the lowest 5th percentile of the measured mixing ratios within a 7-day time window (3.5 days backwards and 3.5 days forward) at each measurement point. This 7-day window was carefully selected to capture regional background variability while minimizing short-term fluctuations, ensuring that the background reflects broader regional conditions rather than localized influences.

3. Results and Discussion

3.1. Atmospheric Observations of Methane and Ethane

Throughout the campaign, we recorded an average methane mixing ratio of 2005 ± 77 ppb, which is 98 ppb higher than the average observed during the AQABA campaign in the summer of 2017 (Paris et al., 2021). Considering the global methane growth rate of 65 ppb from 2018 to 2022 (NOAA, <https://gml.noaa.gov>), this discrepancy may be due to seasonally higher mixing ratios during winter for the northern hemisphere, increased regional emissions, or differences in air mass origins, and hence source regions sampled.

Throughout the campaign, elevated methane levels were consistently measured over the Atlantic Ocean and Mediterranean Sea, under the influence of air masses from southern European countries such as Portugal, Spain, France, and Italy (Figures 1 and 2). However, ethane mixing ratios remained low over these regions, with the median value for the Mediterranean Sea even falling below that of the Atlantic Ocean (0.63 vs. 0.89 ppb, respectively). This disparity likely reflects aged anthropogenic methane emissions, as ethane has a markedly shorter atmospheric lifetime (ca. 1–2 months), even during winter (Li et al., 2022).

Sailing across the Suez region, we recorded the highest methane (2 852 ppb) and ethane (18.1 ppb) mixing ratios. This region exhibited particularly high mixing ratios and signal variability for all trace gases monitored on board the research vessel, marking it as a pollution hotspot. According to the associated back trajectories, the sampled air masses were influenced by winds from the Bosphorus Strait carrying pollution from as far as Istanbul, presenting a complex mixture of long-range transported and freshly emitted pollutants.

The high methane and ethane levels persisted when crossing the northernmost Red Sea (Figure 2), with back trajectories suggesting the dilution of the local emissions farther downwind the Red Sea. Conversely, the lowest methane mixing ratios were observed in the southern Red Sea (1 949 ppb) when air masses originated from the southern Arabian Peninsula. From this region onward, there was a gradual increase in both methane and ethane levels (Figure 2).

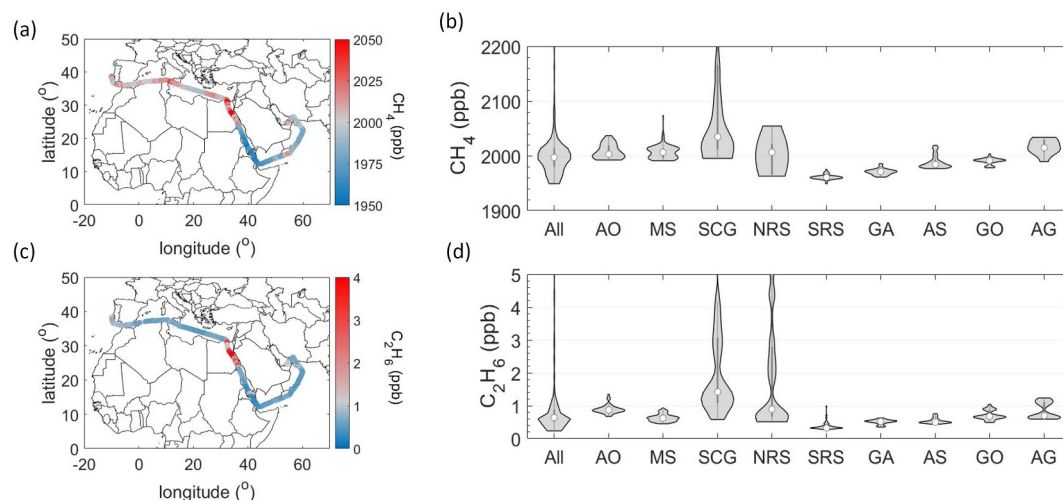


Figure 2. Atmospheric observations of methane (top) and ethane (bottom). (a) Spatial distribution of methane. (b) Regionally segregated violin plots of methane mixing ratios, where the distribution of individual data points is indicated by gray shaded areas, median values by white circles, and 25%–75% range by the black boxplots. (c) Regionally segregated distribution of ethane. (d) Sectoral violin plots of ethane mixing ratios employ the same visual representation as in part (b). The geographical regions are Atlantic Ocean (AO), Mediterranean Sea (MS), Suez Canal and Gulf of Suez (SCG), Northern Red Sea (NRS), Southern Red Sea (SRS), Gulf of Aden (GA), Arabian Sea (AS), Gulf of Oman (GO), and Arabian Gulf (AG).

3.2. Comparison Between Observations and Simulations

3.2.1. Spatial Intercomparison for EDGAR and ECLIPSE

To evaluate the regional methane emissions more accurately, we used excess mixing ratios ($[\Delta\text{CH}_4]$), which involved adjusting the observed data by removing the background levels and comparing them with the simulated excess. This technique sheds light on the intensity of the emissions and underscores the distinct characteristics of each source. It has been frequently employed in emission source characterization at urban (Wennberg et al., 2012), regional (Kille et al., 2019; Paris et al., 2021), and global scales (Irakulis-Loitxate et al., 2021; Weber et al., 2019), using both *in situ* and satellite observations. While this approach does not account for the atmospheric sink of methane due to reactions with hydroxyl radicals (OH), targeting nearby emissions justifies its use as an effective tool for evaluating the emission inventories included in the atmospheric transport model. Thus, we chose to utilize $[\Delta\text{CH}_4]$ for a comparative assessment between observations and simulations. The latest incorporates geospatial emission data from the EDGAR and ECLIPSE inventories, providing a basis for intercomparison along the ship route (Figure 3).

Considering the full range of the observational and simulated data, the average excess mixing ratios showed relatively good consistency, falling within their respective standard deviations ($[\Delta\text{CH}_4]_{\text{obs.}} = 22 \pm 44$ ppb $[\Delta\text{CH}_4]_{\text{EDGAR}} = 27 \pm 22$ ppb $[\Delta\text{CH}_4]_{\text{ECLIPSE}} = 36 \pm 39$ ppb). The observational excess was the lowest among these three data sets, but its respective standard deviation was the highest, possibly due to nearby emissions that may not be properly reproduced by the models due to dilution within the simulated grid cells for the modeled output.

While simulations with both inventories appeared to adequately reflect the transport of European emissions, notable discrepancies were observed in the eastern Mediterranean Sea and Suez region in both simulations (Figure 3a). Similarly, the results from the Gulf of Aden showed important inconsistencies with EDGAR-based simulations leading to an overestimation of concentrations, whereas ECLIPSE-based simulations appeared much stronger than the actual measurements over the Arabian Sea. Overall, by comparing the ratio between the observed and simulated excess methane, the Southern Red Sea and Gulf of Aden were identified as areas with the largest discrepancies between observations and simulations (Figures 3b and 3c).

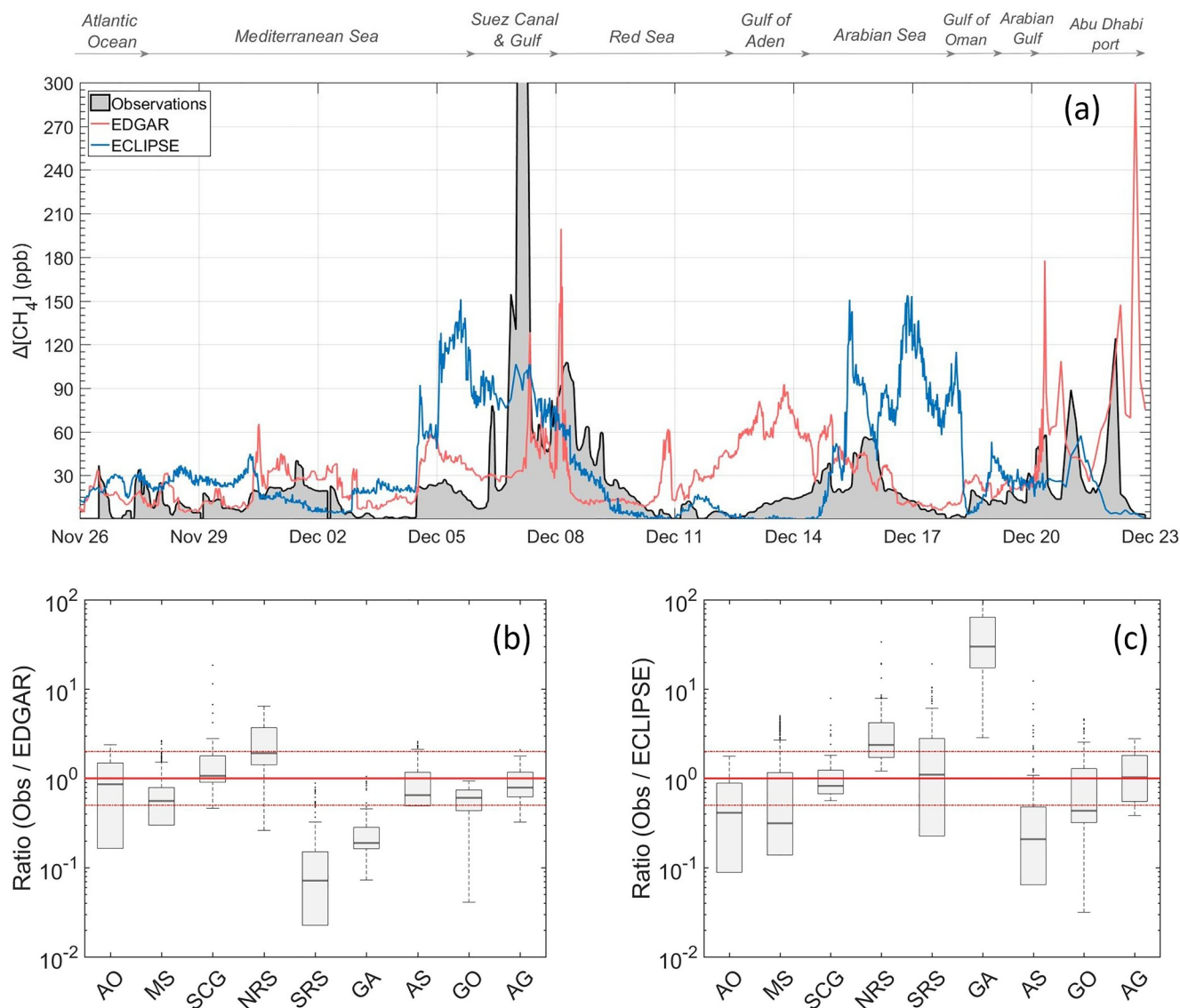


Figure 3. Observed and simulated excess methane mixing ratios. (a) Timeseries of observations (black line with gray shaded area) and simulations using the Emissions Database for Global Atmospheric Research (EDGAR) (red) and ECLIPSE (blue) emission inventories. The ratio between observations and simulations for EDGAR (b) and ECLIPSE (c) is plotted together with the 1:1 (thick red line) and the 2:1 and 1:2 ratios (dashed red lines). On each box, the center line (red) indicates the median, and the bottom and top borders of the box (blue) indicate the 25th and 75th percentiles, respectively. The whiskers extend to the most extreme data points not considered outliers, and the outliers are plotted individually using the dot symbol (black). The abbreviations in b and c are as in Figure 2.

3.2.2. Source and Origin of EDGAR-Based Simulated Methane

To further explore the discrepancies between observed and simulated ΔCH_4 levels, we shifted our focus to the EDGAR-based simulations. These provide comprehensive insights into the documented methane sources and their geographical origins, as illustrated in Figure 4. While the simulations generally matched well with observations for Western European sources, a discrepancy emerged when reaching the easternmost Mediterranean Sea. After this point, we identified two distinct periods (P1 and P2) in which observed methane levels significantly exceeded those predicted by the simulations. These periods occurred over the Suez Canal and Suez Gulf, extending to the northern Red Sea. During P1 and P2, the heightened methane measurements did not match any sources identified in the simulations, indicating either underestimated emission factors or overlooked emission sources.

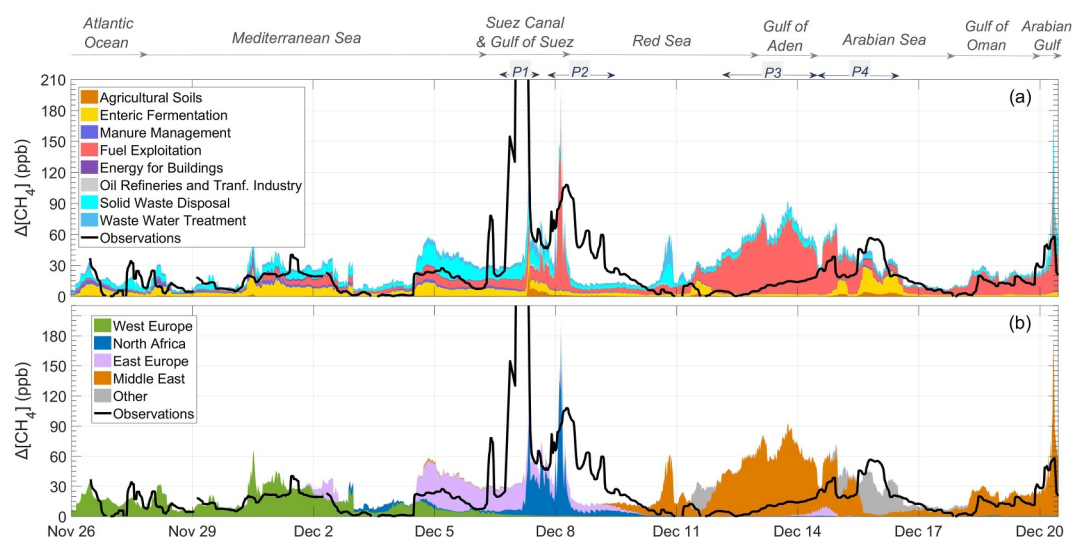


Figure 4. Source and origin of EDGAR-based simulated excess methane. Emission sector (a) and geographical (b) contributions of selected sources are shown with shaded areas. The observed $[\Delta\text{CH}_4]$ is shown with a thick black line in both plots.

Along the southern Red Sea and Gulf of Aden, the simulations indicated a period with long-lasting, strong Middle Eastern emissions that our observations did not capture (P3). Considering the data collected around the Arabian Peninsula (i.e., from the entrance of the Suez Canal to the port of Abu Dhabi), the model attributed approximately $55 \pm 24\%$ of the regional methane emissions to the fuel exploitation sector. This sector is dominated by O&G extraction and processing, and fugitive emissions also play a role, particularly in a region with negligible coal emissions (Scarpelli et al., 2022). Additionally, the model allocated the remaining emissions to enteric fermentation ($16 \pm 14\%$), solid waste landfills ($12 \pm 9\%$), wastewater treatment ($11 \pm 6\%$), manure management ($2 \pm 2\%$), and agricultural soils ($2 \pm 3\%$). The significance of enteric fermentation emissions, as highlighted by the simulations for December 15th and 16th, marked another period of interest, referred to as P4. After organizing the data according to different marine regions and specific periods of interest (P1–P4), we provide a comparative analysis of the observations and simulations for each cluster, as illustrated in Figure S3 in Supporting Information S1.

3.3. Use of NMHCs for Resolving Source Attribution Discrepancies

In this section, we attempt to explain the discrepancies between observations and simulations during the four selected periods when observed methane levels were higher than anticipated (P1, P2, P4) and when simulations significantly overestimated methane levels (P3). Given that most emission sources exhibit characteristic chemical composition patterns, the ratios of hydrocarbons and the relationships between NMHCs and GHGs can then serve as valuable tools for identifying these emission sources.

3.3.1. Suez Canal and Suez Gulf—A Complex Mixture of Sources

Utilizing the isomeric composition of pentane as a diagnostic tool has proven to be effective in differentiating between various emission sources. This method has previously been employed to distinguish emissions from different sources such as O&G (Bourtsoukidis et al., 2019; Gilman et al., 2013; Paris et al., 2021; Swarthout et al., 2013), evaporative losses from gasoline (Gentner et al., 2009), vehicular emissions (Broderick & Mar-nane, 2002; Harley et al., 1992), and a broader spectrum of pollutants characterizing urban atmospheres (Baker et al., 2008; Barletta et al., 2017; Panopoulou et al., 2018; Warneke et al., 2007). Since both isomers react with OH at similar rates (Atkinson et al., 1982), their ratio should remain constant regardless their chemical aging during atmospheric transport. This stability of the ratio allows for accurate source identification even for emissions that have undergone long-range transport (Germain-Piaulenne et al., 2024). Therefore, the distinct emission signature

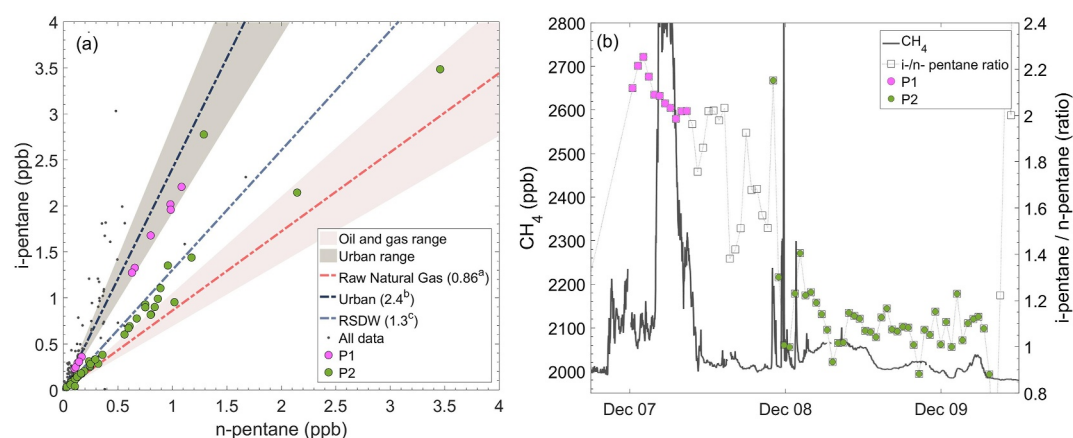


Figure 5. Relationship between pentane isomers for methane source identification. The relationship between i- and n-pentane is shown for two event periods (P1 and P2) in the Suez Canal and Suez Gulf, extending to the Northern Red Sea (see Figure S4 in Supporting Information S1). (a) The linear relationship is plotted with the literature-based emission ratio slopes for raw natural gas^a (Gilman et al., 2013), urban areas^b (Baker et al., 2008), and Red Sea Deep Water^c (Bourtsoukidis et al., 2020). (b) Timeseries of methane mixing ratios (left axis) and i- to n-pentane ratio (right axis).

ratio between the i-pentane and n-pentane isomers can be instrumental in categorizing methane sources in complex polluted environments.

The Suez region had the highest concentrations of all pollutants. As indicated by the simulations presented in Figure 4a, this pattern was attributed to a multitude of regional emission sources. During the first period (P1; from 06 Dec. 9PM to 07 Dec. 9AM UTC), there was a prominent increase in excess methane ($\Delta\text{CH}_4 = 361 \pm 267$ ppb), which was correlated with increases in CO₂, CO, alkanes, and alkenes (Figure S4 in Supporting Information S1). The presence of such high alkene mixing ratios, which are known for their high reactivity and short atmospheric lifetimes, indicates a strong nearby source. Throughout P1, the isomeric pentane ratio averaged at 2.1 ± 0.1 (Figure 5), suggesting urban emission influences along the Suez Canal that previously demonstrated a high load of reactive gases and their oxidation products (Bourtsoukidis et al., 2019; Dienhart et al., 2021; Pfannerstill et al., 2019; Wang et al., 2020). Despite the persistent high pentane ratio for almost 6 hours, the methane peak was comparatively shorter in duration and occurred in the second part of P1. This discrepancy indicates that while the emissions can be linked to urban activities in the vicinity of Port Said, they likely originated from a specific sector that is associated with combustion processes not currently accounted for in emission models (Wang et al., 2020). Therefore, we may hypothesize that this emission source is linked to older marine vessels (Wang et al., 2022), cooking activities along the Suez Canal (Lebel et al., 2022), or open waste burning, a common activity in Egypt that has important implications for the local air quality (Christodoulou et al., 2024).

Along the Suez Canal, the simulated ΔCH_4 was, on average, 3.2 ± 4.4 times lower in the EDGAR-based simulations and 1.7 ± 1.8 times lower in the ECLIPSE-based simulations compared to the observed values, indicating a likely widespread underestimation attributable to anthropogenic emissions. Considering the yearly averaged satellite observations of methane from the Copernicus Sentinel-5P Mapping Portal (<https://maps.s5p-pal.com/ch4/year/>), the Port Said region emerges as a consistent methane hotspot, suggesting that our single transect observations may reflect a systematic bias in the EDGAR inventory. This bias appears to be unrelated to boundary layer dynamics, as indicated by the sharp increase in CH₄ mixing ratios at 4 a.m. (Figure 5b) and the reversed ethane-to-propane ratio, which points to source-based dynamics rather than boundary layer processes as the main driver of this discrepancy between observations and simulations. The start of the second period (P2; from 7 Dec. 10PM to 9 Dec. 8AM UTC) was marked by three methane spikes. The initial one featured a high pentane ratio without a corresponding increase in CO₂ and a spike in alkanes (Figure S4 in Supporting Information S1). The second peak had a pentane ratio of 1 and lower alkene concentrations, both of which are indicative of O&G fugitive emissions. Additionally, the $\Delta\text{C}_2\text{H}_6:\Delta\text{CH}_4$ ratio displayed a higher value during P2, with a mean of 0.04 ± 0.01 , which is another indication supporting the O&G influence (Germain-Piaulenne et al., 2024; Yacovitch et al., 2020). During these samples, Jaywun sampled air from a region known for its oil extraction

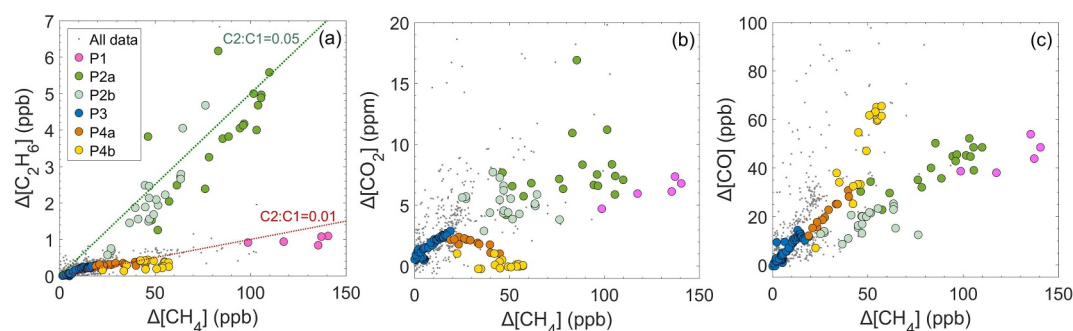


Figure 6. Interspecies relationships of excess mixing ratios for the event periods. Excess ethane (a), carbon dioxide (b), and carbon monoxide (c) are plotted against the excess methane.

activities (El-Magd et al., 2023). This event was reflected in the EDGAR-based model simulation, albeit with a sharper peak and a shorter duration (Figure 4a).

Following the O&G-related event, the pentane isomers exhibited variable ratios (between 1 and 1.3) along with less noisy methane fluctuations, suggesting that P2 could be further divided into two distinct phases (Figure S5 in Supporting Information S1). The initial phase was marked by the above-mentioned methane emissions related to oil exploitation. In contrast, the second phase was characterized by weaker ethane–methane correlations and two minor methane peaks. These peaks, occurring over the Oceanographer and Kebrit brine pools, coincided with the recently identified Red Sea Deep Water (RSDW) hydrocarbon source (Bourtsoukidis et al., 2020), pointing out marine-oriented emissions. This source identification is further supported by the pentane ratio having a steeper slope, the absence of alkenes and CO_2 , and the weak relationship with CO for most samples. Thus, P2 featured a complex blend of emissions that included urban sources in the early phase (P2a) and, later, recent natural emissions from the RSDW along with transported emissions from the Gulf of Suez (P2b).

3.3.2. Long-Range Transport of Emissions From Fuel Exploitation and Agriculture

Sailing southward, the measured ΔCH_4 decreased, eventually aligning with the background conditions, as demonstrated by the marginal ΔCH_4 values, over the southernmost Red Sea. Beyond this point, methane levels started to rise steadily over the Gulf of Aden and throughout much of the Arabian Sea until they returned to background levels over the Gulf of Oman. This part of the track is split into two periods (P3 and P4), marked in Figure 4, which appears to be influenced by emissions transported from the Middle East and West Asia, respectively.

The third period (P3; from 12 Dec. 0 AM to 14 Dec. 12 AM UTC) exhibited high simulated methane, attributed to emissions from the Middle East ($97.5 \pm 2.8\%$), with a significant portion ($82.2 \pm 3.7\%$) linked to the O&G sector. However, the measured ΔCH_4 was significantly lower than the simulated one, averaging a mere increase of 8.6 ± 5.3 ppb marking a ca. sevenfold overestimation in contrast to the predicted 60.1 ± 13.5 ppb. As for NMHCs, P3 had low levels of alkanes and a complete absence of alkenes, which is indicative of chemically processed air masses. The marginal increase in the mixing ratios for all gases over background conditions (Figure 6) was also characterized by a low ratio of ethane to methane ($\Delta\text{C}_2\text{H}_6:\Delta\text{CH}_4 < 0.01$ ppb ppb⁻¹). The markedly different behavior of P3 compared to the O&G-related P2a cluster along with the high confidence in air mass origins (Figure S2 in Supporting Information S1), correlation with ΔCO_2 , and distinctive characteristics of the NMHC emission signature strongly indicate that the EDGAR emission inventory significantly overestimated the long-range transported methane emissions from fuel exploitation activities during P3.

The fourth period encompasses two distinct time segments that, while sharing some similarities, originate from different geographical regions (Figure S6 in Supporting Information S1). The initial segment (P4a; from 14 Dec. 12AM to 15 Dec. 00AM UTC) was predominantly influenced by the Middle East ($79.9 \pm 6.7\%$), with a large contribution from the O&G sector ($82.6 \pm 7.4\%$) and minimal impact from other areas (ca. 7%). The second segment (P4b; from 15 Dec. 12AM to 16 Dec. 06AM) was influenced by air masses originating from West Asia (ca. 85%), with simulations indicating a notable contribution of methane from enteric fermentation

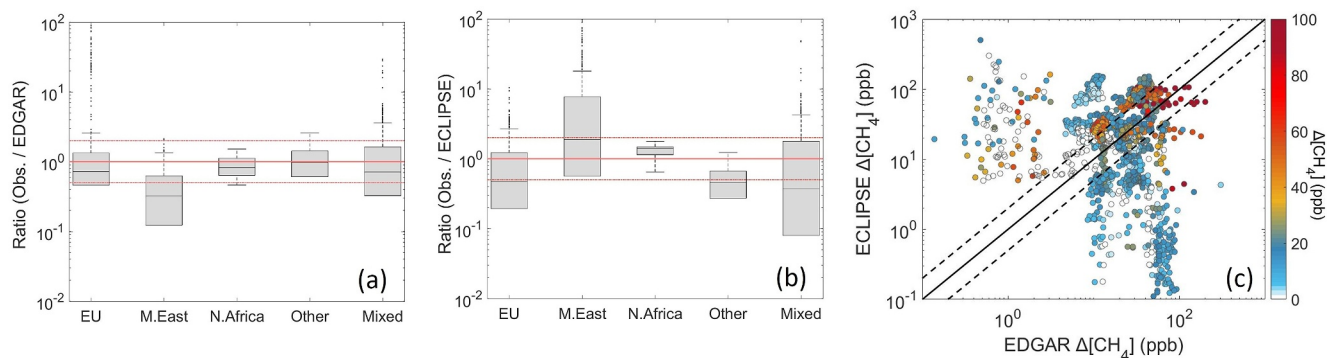


Figure 7. Overview comparison between measured and simulated excess methane mixing ratios. The ratios between observations and the EDGAR-based simulations (a), and ECLIPSE-based simulations (b) are shown as boxplots together with the 1:1 (thick red line) and the 2:1 and 1:2 ratios (dashed red lines). On each box, the center line (black) indicates the median and the bottom and top borders of the box (blue) indicate the 25th and 75th percentiles, respectively. The whiskers extend to the most extreme data points not considered outliers, and the outliers are plotted individually using the dot symbol (black). (c) Three-dimensional comparison between the simulated methane excess by two emission inventories, color-coded with the observed excess. In c, the gray dashed area indicates the majority of the data points that were influenced by Middle Eastern air masses.

($47.6 \pm 10.5\%$). Analyzing the relationships between excess methane, ethane, CO_2 , and CO (Figure 6) can help assess the EDGAR-based source attribution for P4.

Although both segments lacked ethane, their dynamics with the most prevalent greenhouse and trace gases diverged. P4a, which was strongly influenced by Oman and other O&G emissions-dominated countries in the Arabian Peninsula, showed an inverse relationship between ΔCO_2 and ΔCH_4 . This anticorrelation appears to be linked to GHG dynamics driven by the region's diverse ecosystems, ranging from arid desert soils to coastal mangroves. Desert soils, which experience occasional hydration events, harbor microbiomes that influence both methane and CO_2 dynamics (Al-Nadabi & Sulaiman, 2018). Coastal mangroves, subject to saline and tidal conditions, not only emit methane but are also pivotal in CO_2 sequestration (Adame et al., 2021; Cusack et al., 2018). The impact of traditional agricultural practices on soil carbon dynamics can also promote CO_2 uptake through specific cultivation techniques, further complicating this balance (Paustian et al., 1997). Nevertheless, the simulated increase due to O&G emissions does not correspond to the interspecies patterns for this segment, aligning with the general pattern observed for P3, indicating an overestimation of the methane emissions originating from O&G exploitation activities for this part of the ship route.

In contrast, P4b exhibited no correlation with ΔCO_2 , and most data points coincided with ΔCO , and hence, there was no relationship with combustion-related sources. This pattern points toward methane emissions linked to livestock, a significant activity in regions such as Pakistan and India known for their extensive cattle farming (Garg et al., 2011; Habib & Khan, 2018; Ijaz & Goheer, 2021). These relationships among trace gases tend to support the EDGAR-attributed sources, while the comparison of the excess mixing ratios suggests that the contribution from livestock during this event could be slightly underestimated by the inventory.

3.4. Fuel Exploitation Emissions From Middle East—An Uncertainty Hotspot

After detailing the measurement-model discrepancies across the selected periods, this section provides an overview of the relationship between observations and the two sets of simulations. By deriving the ratio between the observed and simulated ΔCH_4 values and illustrating the correlation among all three data sets (Figure 7), this approach can provide valuable information on the extent of agreement between the observations and simulations.

Considering the entire data set, the median ratio between observations and EDGAR-based simulations is 0.62, while the ratio for ECLIPSE-based simulations is slightly higher at 0.65. These values indicate a general overestimation of the simulated methane emissions along the surveyed route. However, the sole use of these ratios cannot be conclusive when assessing the overall accuracy of the simulations as they are heavily influenced by the very low ratios observed in P3 for EDGAR and over the Gulf of Oman for ECLIPSE.

Despite these discrepancies, both models align relatively well with the observations for the European outflow with the majority of the high ΔCH_4 points falling within the 1:2–2:1 ratio range (Figure S7 in Supporting Information S1). This threefold relationship indicates a relatively good performance of the simulations, particularly when considering the challenges associated with measurements taken from a moving platform. Factors such as the precision of the Lagrangian dispersion models (Angevine et al., 2014; Locatelli et al., 2013), the resolution of the grid (Locatelli et al., 2015), and uncertainties related to boundary layer definition (Wu et al., 2005) add further complexity to interpreting these results.

The uncertainties intensify under long-range transported air masses from the Middle East and are linked to O&G exploitation activities. These emissions appear to be significantly overestimated by the EDGAR-based simulations but underestimated by the ECLIPSE-based simulations (Figure S7 in Supporting Information S1). Despite these discrepancies manifesting under conditions of relatively low measured excess methane, the unusual relationships between observations and both EDGAR and ECLIPSE simulations (Figure 3) point to the Middle East, especially its O&G sector, as an “uncertainty hotspot” in methane emission inventories.

4. Conclusions and Perspectives

Shipborne observations of methane and NMHCs were conducted in the marine boundary layer of the Mediterranean Sea and around the Arabian Peninsula, tracing a route from Vigo to Abu Dhabi. To examine the accuracy of regional methane emission inventories, we complemented our observations with Lagrangian dispersion model simulations coupled with two global emission inventories (EDGAR and ECLIPSE). While the measured and simulated methane mixing ratios were in agreement for air masses originating from Europe, notable discrepancies were observed in the eastern and southern parts of Arabian Peninsula, setting the focus of our analyses.

By comparing the measured and EDGAR-based simulated ΔCH_4 , we identified four distinct periods where notable deviations occurred. The localized discrepancies between observations and simulations were partly resolved with the use of NMHC, which appears to be a valuable tool for apportioning the sources of methane emissions at regional scales. Urban sources, compounded by emissions from O&G activities and marine traffic, contributed to the highest concentrations recorded during the campaign, evidencing the Suez region as a pollution hotspot. In a region poised for rapid development, such as the construction of NEOM city in the northeast Red Sea, the combined impact of international marine traffic and various local sources underscores the need for prolonged observations in the Red Sea, the necessity of focused urban air pollution abatement strategies, and the globally relevant decarbonization of marine traffic emissions.

The most significant divergence between the observed and simulated ΔCH_4 occurred over the southern Red Sea, the Gulf of Aden, and the beginning of the Arabian Sea, where air mass back trajectories suggest a widespread emission footprint across the entire Arabian Gulf. Surprisingly, our observations did not capture the long-range transport of methane emissions from the O&G sector, as represented in EDGAR-based simulations. A similar overestimation was detected in the ECLIPSE-based simulations, albeit later in the route, revealing substantial inconsistencies between these emission inventories and actual observations. Despite these challenges, the highest methane observations showed better agreement with the simulations, highlighting the Middle East, particularly the O&G sector, as a critical area of uncertainty in methane emissions.

Given the limitations associated with the sampling duration of this expedition, the scarcity of *in situ*, open-access methane data in the Middle East, and the large uncertainties in satellite-derived emissions for O&G-related sector (Tibrewal et al., 2024), targeted field campaigns in the Arabian Gulf and long-term dense observations emerge as top priorities to better constrain Middle East methane emissions. For effective progress toward mitigating anthropogenic methane emissions and the general decarbonization of the O&G sector in the Middle East, accurate data on GHGs and NMHCs are essential. Such efforts would enhance the accuracy of current emission inventories, validate the satellite-based CH_4 observations, and evaluate the success of measures aimed at reducing methane emissions from this critical sector.

Data Availability Statement

The data sets for methane and non-methane hydrocarbons are openly available at Qu  h   et al. (2024) and Byron et al. (2024), respectively.

Acknowledgments

We express our deepest gratitude toward Shaikha Al Dhaheeri Ahmed Alhashmi, Faisal Al Hammadi, Ahmed Baharoon, Sultan Alhammadi, Sara Almehairbi, Alya Alhosani, and Winston Cowie from the Environment Agency—Abu Dhabi (EAD), owners and operators of the Jaywun research vessel, for the realization of the AREAD campaign that would have not been possible without their contributions. We extend our appreciation to the captain and crew of the Jaywun Research Vessel for providing the best possible working conditions during this campaign. We are particularly grateful to the Technical Research Specialists of the Cyprus Institute, Nikoleta Lekaki and Moreno Parolin, for their contribution to the operation of the analytical instrumentation throughout the journey from Vigo to Abu Dhabi and to Rafail Konatzii, Pantelis Chatzikonstantinou, and Rolf Hofmann for their help during the installation period. We acknowledge the use of www.flexpart.eu for accessing the FLEXPART and FLEX-extract source codes. This work was supported by the European Union's Horizon 2020 research and innovation program (Grant 856612) and the Cyprus Government (EMME-CARE).

References

Adame, M. F., Reef, R., Santini, N. S., Najera, E., Turschwell, M. P., Hayes, M. A., et al. (2021). Mangroves in arid regions: Ecology, threats, and opportunities. *Estuarine, Coastal and Shelf Science*, 248, 106796. <https://doi.org/10.1016/j.ecss.2020.106796>

Allen, D. (2016). Attributing atmospheric methane to anthropogenic emission sources. *Accounts of Chemical Research*, 49(7), 1344–1350. <https://doi.org/10.1021/acs.accounts.6b00081>

Al-Nadabi, A., & Sulaiman, H. (2018). Carbon sink potential of *Avicennia marina* in the Al-Qurm nature reserve, Muscat, Oman. *IOP Conference Series: Earth and Environmental Science*, 151, 012003. <https://doi.org/10.1088/1755-1315/151/1/012003>

Al-Shalal, A., Lowry, D., Fisher, R. E., Nisbet, E. G., Zazzeri, G., Al-Sarawi, M., & France, J. L. (2022). Methane emissions in Kuwait: Plume identification, isotopic characterisation and inventory verification. *Atmospheric Environment*, 268, 118763. <https://doi.org/10.1016/j.atmosenv.2021.118763>

Alvarez, R. A., Zavala-Araiza, D., Lyon, D. R., Allen, D. T., Barkley, Z. R., Brandt, A. R., et al. (2018). Assessment of methane emissions from the U. S. oil and gas supply chain. *Science*, 361(6398), 186–188. <https://doi.org/10.1126/science.aar7204>

Angevine, W. M., Brioude, J., McKeen, S., & Holloway, J. S. (2014). Uncertainty in Lagrangian pollutant transport simulations due to meteorological uncertainty from a mesoscale WRF ensemble. *Geoscientific Model Development*, 7(6), 2817–2829. <https://doi.org/10.5194/gmd-7-2817-2014>

Atkinson, R., Aschmann, S. M., Winer, A. M., & Pitts, J. N. (1982). Rate constants for the reaction of OH radicals with a series of alkanes and alkenes at 299 ± 2 K. *International Journal of Chemical Kinetics*, 14(5), 507–516. <https://doi.org/10.1002/kin.550140508>

Baker, A. K., Beyersdorf, A. J., Doezema, L. A., Katzenstein, A., Meinardi, S., Simpson, I. J., et al. (2008). Measurements of nonmethane hydrocarbons in 28 United States cities. *Atmospheric Environment*, 42(1), 170–182. <https://doi.org/10.1016/j.atmosenv.2007.09.007>

Barletta, B., Simpson, I. J., Blake, N. J., Meinardi, S., Emmons, L. K., Aburizaiza, O. S., et al. (2017). Characterization of carbon monoxide, methane and nonmethane hydrocarbons in emerging cities of Saudi Arabia and Pakistan and in Singapore. *Journal of Atmospheric Chemistry*, 74(1), 87–113. <https://doi.org/10.1007/s10874-016-9343-7>

Berchet, A., Pison, I., & Narbaud, C. (2023). FLEXPART-GUI-toolbox [Object]. <https://doi.org/10.5281/ZENODO.7766371>

Bourtsoukidis, E., Ernle, L., Crowley, J. N., Lelieveld, J., Paris, J.-D., Pozzer, A., et al. (2019). Non-methane hydrocarbon (C2-C8) sources and sinks around the Arabian Peninsula. *Atmospheric Chemistry and Physics*, 19(10), 7209–7232. <https://doi.org/10.5194/acp-19-7209-2019>

Bourtsoukidis, E., Pozzer, A., Sattler, T., Matthaïos, V. N., Ernle, L., Edtbauer, A., et al. (2020). The red sea deep water is a potent source of atmospheric ethane and propane. *Nature Communications*, 11(1), 447. <https://doi.org/10.1038/s41467-020-14375-0>

Broderick, B. M., & Marnane, I. S. (2002). A comparison of the C2–C9 hydrocarbon compositions of vehicle fuels and urban air in Dublin, Ireland. *Atmospheric Environment*, 36(6), 975–986. [https://doi.org/10.1016/S1352-2310\(01\)00472-1](https://doi.org/10.1016/S1352-2310(01)00472-1)

Byron, J., Bourtsoukidis, E., & Williams, J. (2024). Non-methane hydrocarbons (NMHC) during the atmospheric research expedition to Abu Dhabi (AREAD) [Dataset]. <https://doi.org/10.5281/zenodo.11207149>

Chen, L., Zuo, L., Jiang, Z., Jiang, S., Liu, K., Tan, J., & Zhang, L. (2019). Mechanisms of shale gas adsorption: Evidence from thermodynamics and kinetics study of methane adsorption on shale. *Chemical Engineering Journal*, 361, 559–570. <https://doi.org/10.1016/j.cej.2018.11.185>

Christodoulou, A., Bezantakos, S., Bourtsoukidis, E., Stavroulas, I., Pikridas, M., Oikonomou, K., et al. (2024). Submicron aerosol pollution in greater Cairo (Egypt): A new type of urban haze? *Environment International*, 186, 108610. <https://doi.org/10.1016/j.envint.2024.108610>

Cooper, J., Dubey, L., & Hawkes, A. (2022). Methane detection and quantification in the upstream oil and gas sector: The role of satellites in emissions detection, reconciling and reporting. *Environmental Sciences: Atmosphere*, 2(1), 9–23. <https://doi.org/10.1039/D1EA00046B>

Cusack, M., Saderne, V., Arias-Ortiz, A., Masqué, P., Krishnakumar, P. K., Rabaoui, L., et al. (2018). Organic carbon sequestration and storage in vegetated coastal habitats along the western coast of the Arabian Gulf. *Environmental Research Letters*, 13(7), 074007. <https://doi.org/10.1088/1748-9326/aac899>

Dienhart, D., Crowley, J. N., Bourtsoukidis, E., Edtbauer, A., Eger, P. G., Ernle, L., et al. (2021). Measurement report: Observation-based formaldehyde production rates and their relation to OH reactivity around the Arabian Peninsula. *Atmospheric Chemistry and Physics*, 21(23), 17373–17388. <https://doi.org/10.5194/acp-21-17373-2021>

El-Magd, I. A., Zakzouk, M., Ali, E. M., Abdulaziz, A. M., Rehman, A., & Saba, T. (2023). Mapping oil pollution in the Gulf of Suez in 2017–2021 using synthetic aperture radar. *The Egyptian Journal of Remote Sensing and Space Sciences*, 26(3), 826–838. <https://doi.org/10.1016/j.ejrs.2023.08.005>

Fiocco, G., Mastrantonio, G., & Ricotta, A. (1980). Boundary layer structure observed by shipborne Doppler Sodar in the Suez Canal zone. *Il Nuovo Cimento - B C*, 3(4), 321–344. <https://doi.org/10.1007/BF02510159>

Garg, A., Kankal, B., & Shukla, P. R. (2011). Methane emissions in India: Sub-regional and sectoral trends. *Atmospheric Environment*, 45(28), 4922–4929. <https://doi.org/10.1016/j.atmosenv.2011.06.004>

Gentner, D. R., Harley, R. A., Miller, A. M., & Goldstein, A. H. (2009). Diurnal and seasonal variability of gasoline-related volatile organic compound emissions in riverside, California. *Environmental Science & Technology*, 43(12), 4247–4252. <https://doi.org/10.1021/es9006228>

Germain-Piaulenne, E., Paris, J.-D., Gros, V., Quéhé, P.-Y., Pikridas, M., Baisnée, D., et al. (2024). Middle East oil and gas methane emissions signature captured at a remote site using light hydrocarbon tracers. *Atmospheric Environment X*, 22, 100253. <https://doi.org/10.1016/j.aeoa.2024.100253>

Gilman, J. B., Lerner, B. M., Kuster, W. C., & De Gouw, J. A. (2013). Source signature of volatile organic compounds from oil and natural gas operations in northeastern Colorado. *Environmental Science & Technology*, 47(3), 1297–1305. <https://doi.org/10.1021/es304119a>

Habib, G., & Khan, A. A. (2018). Assessment and mitigation of methane emissions from livestock sector in Pakistan. *Earth Systems and Environment*, 2(3), 601–608. <https://doi.org/10.1007/s41748-018-0076-4>

Harley, R. A., Hannigan, M. P., & Cass, G. R. (1992). Respeciation of organic gas emissions and the detection of excess unburned gasoline in the atmosphere. *Environmental Science & Technology*, 26(12), 2395–2408. <https://doi.org/10.1021/es00036a010>

Höglund-Isaksson, L. (2012). Global anthropogenic methane emissions 2005–2030: Technical mitigation potentials and costs. *Atmospheric Chemistry and Physics*, 12(19), 9079–9096. <https://doi.org/10.5194/acp-12-9079-2012>

Iea, P. (2024). *Global methane tracker 2024*. IEA. Retrieved from <https://www.iea.org/reports/global-methane-tracker-2024>

Ijaz, M., & Goheer, M. A. (2021). Emission profile of Pakistan's agriculture: Past trends and future projections. *Environment, Development and Sustainability*, 23(2), 1668–1687. <https://doi.org/10.1007/s10668-020-00645-w>

Irakulis-Loitxate, I., Guanter, L., Liu, Y.-N., Varon, D. J., Maasakkers, J. D., Zhang, Y., et al. (2021). Satellite-based survey of extreme methane emissions in the Permian basin. *Science Advances*, 7(27), eabf4507. <https://doi.org/10.1126/sciadv.abf4507>

Janssens-Maenhout, G., Crippa, M., Guizzardi, D., Muntean, M., Schaaf, E., Dentener, F., et al. (2019). EDGAR v4.3.2 Global Atlas of the three major greenhouse gas emissions for the period 1970–2012. *Earth System Science Data*, 11(3), 959–1002. <https://doi.org/10.5194/essd-11-959-2019>

- Karion, A., Lauvaux, T., Lopez Coto, I., Sweeney, C., Mueller, K., Gourdji, S., et al. (2019). Intercomparison of atmospheric trace gas dispersion models: Barnett Shale case study. *Atmospheric Chemistry and Physics*, 19(4), 2561–2576. <https://doi.org/10.5194/acp-19-2561-2019>
- Kille, N., Chiu, R., Frey, M., Hase, F., Sha, M. K., Blumenstock, T., et al. (2019). Separation of methane emissions from agricultural and natural gas sources in the Colorado front range. *Geophysical Research Letters*, 46(7), 3990–3998. <https://doi.org/10.1029/2019GL082132>
- Lebel, E. D., Finnegan, C. J., Ouyang, Z., & Jackson, R. B. (2022). Methane and NO_x emissions from natural gas stoves, cooktops, and ovens in residential homes. *Environmental Science & Technology*, 56(4), 2529–2539. <https://doi.org/10.1021/acs.est.1c04707>
- Lee, H., Calvin, K., Dasgupta, D., Krinner, G., Mukherji, A., Thorne, P. W., et al. (2023). IPCC, 2023: Climate change 2023: Synthesis report. In H. Lee & J. Romero (Eds.), *Contribution of working groups I, II and III to the sixth assessment report of the intergovernmental panel on climate change [core writing team]*. IPCC. Intergovernmental Panel on Climate Change (IPCC). <https://doi.org/10.59327/IPCC/AR6-9789291691647>
- Li, M., Pozzer, A., Lelieveld, J., & Williams, J. (2022). Northern Hemispheric atmospheric ethane trends in the upper troposphere and lower stratosphere (2006–2016) with reference to methane and propane. *Earth System Science Data*, 14(9), 4351–4364. <https://doi.org/10.5194/essd-14-4351-2022>
- Locatelli, R., Bousquet, P., Chevallier, F., Fortems-Cheney, A., Szopa, S., Saunio, M., et al. (2013). Impact of transport model errors on the global and regional methane emissions estimated by inverse modelling. *Atmospheric Chemistry and Physics*, 13(19), 9917–9937. <https://doi.org/10.5194/acp-13-9917-2013>
- Locatelli, R., Bousquet, P., Saunio, M., Chevallier, F., & Cressot, C. (2015). Sensitivity of the recent methane budget to LMDz sub-grid-scale physical parameterizations. *Atmospheric Chemistry and Physics*, 15(17), 9765–9780. <https://doi.org/10.5194/acp-15-9765-2015>
- Maasakkers, J. D., Jacob, D. J., Sulprizio, M. P., Scarpelli, T. R., Nessler, H., Sheng, J.-X., et al. (2019). Global distribution of methane emissions, emission trends, and OH concentrations and trends inferred from an inversion of GOSAT satellite data for 2010–2015. *Atmospheric Chemistry and Physics*, 19(11), 7859–7881. <https://doi.org/10.5194/acp-19-7859-2019>
- McNorton, J., Wilson, C., Gloor, M., Parker, R. J., Boesch, H., Feng, W., et al. (2018). Attribution of recent increases in atmospheric methane through 3-D inverse modelling. *Atmospheric Chemistry and Physics*, 18(24), 18149–18168. <https://doi.org/10.5194/acp-18-18149-2018>
- Ocko, I. B., Sun, T., Shindell, D., Oppenheimer, M., Hristov, A. N., Pacala, S. W., et al. (2021). Acting rapidly to deploy readily available methane mitigation measures by sector can immediately slow global warming. *Environmental Research Letters*, 16(5), 054042. <https://doi.org/10.1088/1748-9326/abf9c8>
- OPEC. (2020). Annual statistical bulletin 2020, organization of the petroleum exporting countries. Retrieved from https://www.opec.org/opec_web/static_files_project/media/downloads/publications/AR%202020.pdf
- Osipov, S., Chowdhury, S., Crowley, J. N., Tadic, I., Drewnick, F., Borrmann, S., et al. (2022). Severe atmospheric pollution in the Middle East is attributable to anthropogenic sources. *Communications Earth & Environment*, 3(1), 203. <https://doi.org/10.1038/s43247-022-00514-6>
- Panopoulou, A., Liakakou, E., Gros, V., Sauvage, S., Locoge, N., Bonsang, B., et al. (2018). Non-methane hydrocarbon variability in Athens during wintertime: The role of traffic and heating. *Atmospheric Chemistry and Physics*, 18(21), 16139–16154. <https://doi.org/10.5194/acp-18-16139-2018>
- Paris, J.-D., Riandet, A., Boutsoukidis, E., Delmotte, M., Berchet, A., Williams, J., et al. (2021). Shipborne measurements of methane and carbon dioxide in the Middle East and Mediterranean areas and the contribution from oil and gas emissions. *Atmospheric Chemistry and Physics*, 21(16), 12443–12462. <https://doi.org/10.5194/acp-21-12443-2021>
- Parrish, D. D., Stohl, A., Forster, C., Atlas, E. L., Blake, D. R., Goldan, P. D., et al. (2007). Effects of mixing on evolution of hydrocarbon ratios in the troposphere. *Journal of Geophysical Research*, 112(D10), 2006JD007583. <https://doi.org/10.1029/2006JD007583>
- Paustian, K., Andr n, O., Janzen, H. H., Lal, R., Smith, P., Tian, G., et al. (1997). Agricultural soils as a sink to mitigate CO₂ emissions. *Soil Use & Management*, 13(s4), 230–244. <https://doi.org/10.1111/j.1475-2743.1997.tb00594.x>
- Pfannerstill, E. Y., Wang, N., Edtbauer, A., Boutsoukidis, E., Crowley, J. N., Dienhart, D., et al. (2019). Shipborne measurements of total OH reactivity around the Arabian Peninsula and its role in ozone chemistry. *Atmospheric Chemistry and Physics*, 19(17), 11501–11523. <https://doi.org/10.5194/acp-19-11501-2019>
- Qu h , P.-Y., Paris, J.-D., Hazan, L., Boutsoukidis, E., & Sciare, J. (2024). Greenhouse gas (GHG) during the atmospheric research expedition to Abu Dhabi (AREAD) [Dataset]. *Zenodo*. <https://doi.org/10.5281/zenodo.10960263>
- Rella, C. W., Chen, H., Andrews, A. E., Filges, A., Gerbig, C., Hatakkaj, J., et al. (2013). High accuracy measurements of dry mole fractions of carbon dioxide and methane in humid air. *Atmospheric Measurement Techniques*, 6(3), 837–860. <https://doi.org/10.5194/amt-6-837-2013>
- Saunio, M., Martinez, A., Poulter, B., Zhang, Z., Raymond, P., Regnier, P., et al. (2024). Global methane budget 2000–2020. *Earth System Science Data Discussions*, 2024, 1–147. <https://doi.org/10.5194/essd-2024-115>
- Scarpelli, T. R., Jacob, D. J., Grossman, S., Lu, X., Qu, Z., Sulprizio, M. P., et al. (2022). Updated Global Fuel Exploitation Inventory (GFEI) for methane emissions from the oil, gas, and coal sectors: Evaluation with inversions of atmospheric methane observations. *Atmospheric Chemistry and Physics*, 22(5), 3235–3249. <https://doi.org/10.5194/acp-22-3235-2022>
- Schwietzke, S., Sherwood, O. A., Bruhwiler, L. M. P., Miller, J. B., Etiope, G., Dlugokencky, E. J., et al. (2016). Upward revision of global fossil fuel methane emissions based on isotope database. *Nature*, 538(7623), 88–91. <https://doi.org/10.1038/nature19797>
- Stavert, A. R., Saunio, M., Canadell, J. G., Poulter, B., Jackson, R. B., Regnier, P., et al. (2022). Regional trends and drivers of the global methane budget. *Global Change Biology*, 28(1), 182–200. <https://doi.org/10.1111/gcb.15901>
- Stohl, A., Forster, C., Frank, A., Seibert, P., & Wotawa, G. (2005). Technical note: The Lagrangian particle dispersion model FLEXPART version 6.2. *Atmospheric Chemistry and Physics*, 5(9), 2461–2474. <https://doi.org/10.5194/acp-5-2461-2005>
- Swarthout, R. F., Russo, R. S., Zhou, Y., Hart, A. H., & Sive, B. C. (2013). Volatile organic compound distributions during the NACHTT campaign at the boulder atmospheric observatory: Influence of urban and natural gas sources. *Journal of Geophysical Research: Atmospheres*, 118(18). <https://doi.org/10.1002/jgrd.50722>
- Tibrewal, K., Ciais, P., Saunio, M., Martinez, A., Lin, X., Thanwerdas, J., et al. (2024). Assessment of methane emissions from oil, gas and coal sectors across inventories and atmospheric inversions. *Communications Earth & Environment*, 5(1), 26. <https://doi.org/10.1038/s43247-023-01190-w>
- Turner, A. J., Frankenberg, C., & Kort, E. A. (2019). Interpreting contemporary trends in atmospheric methane. *Proceedings of the National Academy of Sciences* (Vol. 116(8), pp. 2805–2813). <https://doi.org/10.1073/pnas.1814297116>
- Upadhyay, A., Dey, S., & Goyal, P. (2020). A comparative assessment of regional representativeness of EDGAR and ECLIPSE emission inventories for air quality studies in India. *Atmospheric Environment*, 223, 117182. <https://doi.org/10.1016/j.atmosenv.2019.117182>
- Wang, L., Du, W., Shen, H., Chen, Y., Zhu, X., Yun, X., et al. (2022). Unexpected methane emissions from old small fishing vessels in China. *Frontiers in Environmental Science*, 10, 907868. <https://doi.org/10.3389/fenvs.2022.907868>
- Wang, N., Edtbauer, A., St nner, C., Pozzer, A., Boutsoukidis, E., Erml, L., et al. (2020). Measurements of carbonyl compounds around the Arabian Peninsula: Overview and model comparison. *Atmospheric Chemistry and Physics*, 20(18), 10807–10829. <https://doi.org/10.5194/acp-20-10807-2020>

- Warneke, C., McKeen, S. A., De Gouw, J. A., Goldan, P. D., Kuster, W. C., Holloway, J. S., et al. (2007). Determination of urban volatile organic compound emission ratios and comparison with an emissions database. *Journal of Geophysical Research*, *112*(D10), 2006JD007930. <https://doi.org/10.1029/2006JD007930>
- Weber, T., Wiseman, N. A., & Kock, A. (2019). Global ocean methane emissions dominated by shallow coastal waters. *Nature Communications*, *10*(1), 4584. <https://doi.org/10.1038/s41467-019-12541-7>
- Wennberg, P. O., Mui, W., Wunch, D., Kort, E. A., Blake, D. R., Atlas, E. L., et al. (2012). On the sources of methane to the Los Angeles atmosphere. *Environmental Science & Technology*, *46*(17), 9282–9289. <https://doi.org/10.1021/es301138y>
- Wilde, S. E., Dominutti, P. A., Allen, G., Andrews, S. J., Bateson, P., Bauguutte, S. J.-B., et al. (2021). Speciation of VOC emissions related to offshore North Sea oil and gas production. *Atmospheric Chemistry and Physics*, *21*(5), 3741–3762. <https://doi.org/10.5194/acp-21-3741-2021>
- Wu, W., Lynch, A. H., & Rivers, A. (2005). Estimating the uncertainty in a regional climate model related to initial and lateral boundary conditions. *Journal of Climate*, *18*(7), 917–933. <https://doi.org/10.1175/JCLI-3293.1>
- Yacovitch, T. I., Daube, C., & Herndon, S. C. (2020). Methane emissions from offshore oil and gas platforms in the Gulf of Mexico. *Environmental Science & Technology*, *54*(6), 3530–3538. <https://doi.org/10.1021/acs.est.9b07148>
- Yver Kwok, C., Laurent, O., Guemri, A., Philippon, C., Wastine, B., Rella, C. W., et al. (2015). Comprehensive laboratory and field testing of cavity ring-down spectroscopy analyzers measuring H₂O, CO₂, CH₄ and CO. *Atmospheric Measurement Techniques*, *8*(9), 3867–3892. <https://doi.org/10.5194/amt-8-3867-2015>
- Zavala-Araiza, D., Lyon, D. R., Alvarez, R. A., Davis, K. J., Harriss, R., Herndon, S. C., et al. (2015). Reconciling divergent estimates of oil and gas methane emissions. *Proceedings of the National Academy of Sciences* (Vol. 112(51), pp. 15597–15602). <https://doi.org/10.1073/pnas.1522126112>
- Zittis, G., Almazroui, M., Alpert, P., Ciais, P., Cramer, W., Dahdal, Y., et al. (2022). Climate change and weather extremes in the eastern mediterranean and Middle East. *Reviews of Geophysics*, *60*(3), e2021RG000762. <https://doi.org/10.1029/2021RG000762>